Synthesis and Properties of Polystyrene–Clay Nanocomposites via *In Situ* Intercalative Polymerization

Rongrong Qi, Xing Jin, Jinghui Nie, Wei Yu, Chixing Zhou

School of Chemistry and Chemical Engineering, Shanghai Jiao Tong University, Shanghai 200240, China

Received 13 January 2004; accepted 22 November 2004
DOI 10.1002/app.21747
Published online in Wiley InterScience (www.interscience.wiley.com).

ABSTRACT: Organophilic montmorillonite (MMT) was prepared by ion exchange between Na^+ ions in the clay and twin benzyldimethyloctadecylammonium bromine cations in an aqueous medium. The organophilic MMT particles were easily dispersed and swollen in styrene monomer. Polystyrene–MMT nanocomposites were prepared by the free-radical polymerization of styrene containing dispersed clay. The intercalation spacing in the nanocomposites and the degree of dispersion of these composites were investigated with X-ray diffraction and transmission electron microscopy, respectively. The nanocomposites had higher weight-average molecular weights, lower glass-transition temperatures, and better thermal stability (the decomposition temperature was improved by ca. 70°C) than the virgin polystyrene. The rheological behavior of the polystyrene–MMT nanocomposites was also studied. © 2005 Wiley Periodicals, Inc. J Appl Polym Sci 97: 201–207, 2005

Key words: nanocomposites; polystyrene; clay

INTRODUCTION

Polymer–inorganic hybrids, based on the intercalation of polymer chains into layered silicates, form a class of nanocomposites that have recently received considerable attention from both academia and industry as an effective means of overcoming the shortcomings of conventional mineral-filled composites.[1,2] The dimensions and microstructure of the dispersed phase significantly influence the properties of polymer composites. In such nanocomposites, the interfacial effect between the silicate layers and matrix polymers is a key factor. However, the hydrophilic nature of clay does not afford its good dispersion in an organic polymer phase. It is essential to improve the interaction between the clay and polymer matrix to produce a useful polymer nanocomposite. Layered silicates have been widely investigated, probably because the starting clay materials are easily obtained and because their intercalation chemistry has been studied for a long time.[3,4] Because of the nanometer-size particles obtained by dispersion, these nanocomposites exhibit markedly improved mechanical, thermal, optical, and physicochemical properties in comparison with those of the pure polymer or conventional (microscale) composites.[1,2,5,6]

As one of the common polymers, polystyrene (PS) has been widely used, and several attempts at preparing PS–clay composites have been reported,[7–15] such as melt intercalation and polymerized intercalation. A common technique involves the impregnation of clay into styrene monomer and subsequent polymerization, but the hydrophilic nature of the untreated clay impedes its homogeneous dispersion in the polymer matrix.[7,8] Akelah and Moet[10] modified the interlayer of sodium montmorillonite (Na-MMT) and calcium montmorillonite by exchanging the inorganic cations with (vinyl benzyl)trimethyl ammonium chloride, but PS–clay intercalated composites with a maximum basal spacing of 2.45 nm were prepared with a solvent (acetonitrile). Doh and Cho[12] prepared intercalated nanocomposites that exhibited higher a decomposition temperature (45°C higher than that of virgin PS), and Fu and Qutubuddin[13] obtained exfoliated nanocomposites with a higher dynamic modulus. In this polymerization intercalation process, some vortex or sonic stirring for a long time is necessary.

In this study, we prepared PS–montmorillonite (MMT) nanocomposites by the free-radical polymerization of styrene containing dispersed clay in the static state. After an appropriate amount of montmorillonite modified with twin benzyldimethyloctadecylammonium bromine (TBDO-MMT) was mixed with the styrene monomer for 10 min, PS–MMT nanocomposites were obtained with free-radical polymerization at 80°C for 72 h. The structure, weight-average molecular weight (M_w), thermal stability, rheological behavior, and glass-transition temperature (T_g) of the nanocomposites were also studied.

Correspondence to: R. Qi (rrqi@sjtu.edu.cn).
Contract grant sponsor: National Science Foundation of China; contract grant number: 50390090.

Materials

MMT and organophilic MMT were kindly supplied by Huate Co., Ltd. (Linan, China). The cation-exchange capacity was approximately 85–110 mequiv/100 g of MMT. Organophilic MMT was prepared by cation exchange between Na^+ in clay galleries and twin benzyldimethyloctadecylammonium bromine (TBDO) cations in an aqueous solution. Styrene (Shanghai Chemical Solvent Co., Ltd., Shanghai, China) was purified by distillation under reduced pressure at 30°C. Benzoyl peroxide (BPO; Shanghai Lingfeng Chemical Solvent Factory, Shanghai, China) was purified by crystallization from chloroform at room temperature.

Synthesis of the PS–clay nanocomposites

The desired amounts of TBDO-MMT and BPO were dispersed and swollen in the styrene monomer. The mixture was stirred for 10 min. The samples were purged with nitrogen for about 15 min and polymerized in an oil bath at 80°C for 72 h to obtain PS–clay nanocomposites. The polymerized PS/TBDO-MMT sample was removed from the flask, crushed, and dried *in vacuo* at 80°C for 24 h. The virgin PS was also prepared according to the aforementioned polymerized conditions.

Characterization of the PS–clay nanocomposites

X-ray diffraction (XRD) patterns were obtained with a Philips PW1710 X-ray diffractometer (Holland) equipped with a Ni-filtered Cu Kα source. The voltage and current of the X-ray tubes were 40 kV and 100 mA, respectively. The basal spacing of MMT was estimated from the position of the (001) peak in the XRD pattern.

The microstructure of the nanocomposites was imaged with a JEM 1200EX transmission electron microscope (JEOL Ltd., Japan); the ultrathin film was cut under cryogenic conditions with a Reichert-Jung Ultracut E microtome (Germany).

Properties of the PS–clay nanocomposites

The samples dissolved in tetrahydrofuran were analyzed by gel permeation chromatography (GPC; PE-GPC200) (PerkinElmer, Norwalk, CT). A refraction-index detector and a 10-μm Mixex-A column gel (PerkinElmer) were used.

The T_g values of the samples were measured with a PerkinElmer Pyris-1 differential scanning calorimeter (PerkinElmer). The transition temperatures were calibrated with indium and zinc standards. All differential scanning calorimetry (DSC) measurements were performed under an inert (N_2) atmosphere at a heating rate of 10°C/min, and samples of approximately 3–5 mg were cut.

The thermal stability analysis was performed with a PerkinElmer TGA7 thermogravimetric analyzer at a heating rate of 20°C/min under a nitrogen or air atmosphere.

The rheological and viscoelastic properties of the melts were obtained with a rotational rheometer (Bohlin Gemini 200HR Rheometrics dynamic stress rheometer, Bohlin Instrument Co., Ltd., UK). The steady-shear viscosities (η) were measured at 250°C. The rheological properties of the virgin PS and PS/TBDO-MMT nanocomposites were measured with 25-mm-diameter parallel plates in the oscillatory shear mode. The dynamic storage modulus (G') and loss modulus (G'') were determined as a function of the angular frequency (ω) with a strain of 0.5% at 250°C. The frequency range was 0.01–100 rad/s. A fixed strain of 0.5% was used to ensure that the measurements were taken within the linear viscoelastic regime of the materials. Tests were carried out in an atmosphere of hot air inside an environmental chamber surrounding the testing fixture. All measurements were carried out under conditions sufficient to guarantee sample stability; the polymer degradation was checked after repeated measurements.

RESULTS AND DISCUSSION

The crystal structure of MMT consists of two-dimensional layers formed by the fusion of two silica tetrahedral sheets to an edge-shared octahedral sheet of aluminum hydroxide. The stacking of the layers of primary clay particles is held together by weak dipolar or van der Waals forces.[16] XRD analysis is a powerful tool for examining the crystal structure of polymer–clay nanocomposites. Figure 1 shows a series of XRD patterns of Na-MMT [Fig. 1(a)], TBDO-MMT [Fig. 1(b)], and PS–clay nanocomposites [Fig. 1(c–g)] and the corresponding patterns of the nanocomposites in the range of the diffraction angle (2θ = 1–30°). The mean interlayer spacings of the (001) plane (d_{001}) were calculated with Bragg's equation, $d = \lambda/(2 \sin \theta)$, where λ is the wavelength of the X-ray, at peak positions. λ was 1.5418 Å. d_{001} for MMT, TBDO-MMT, and the nanocomposites was 14.7, 30.6, and 37.7 Å, respectively. In comparison with the initial interlayer spacing of pristine MMT, it indicates gallery expansions of 16.1 and 23.0 Å, respectively. The large expansion of the gallery may indicate the intercalation of MMT layers by TBDO and PS. The XRD patterns also show that the intensity of the (001) reflection peak of the PS–clay nanocomposites reached its maximum when the concentration of TBDO-MMT was approximately 5 wt %; then it clearly decreased with increasing TBDO-MMT loading. This apparent decrease may be attributed to the formation of partially exfoliated and par-

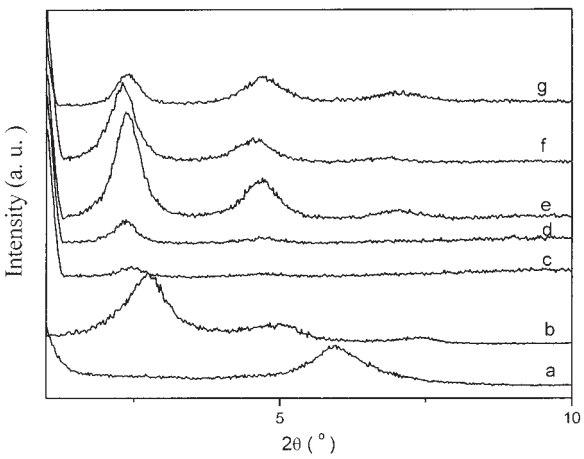

Figure 1 XRD patterns of the samples: (a) Na-MMT, (b) TBDO-MMT, (c) a PS–clay nanocomposite containing 1 wt % TBDO-MMT, (d) a PS–clay nanocomposite containing 3 wt % TBDO-MMT, (e) a PS–clay nanocomposite containing 5 wt % TBDO-MMT, (f) a PS–clay nanocomposite containing 8 wt % TBDO-MMT, and (g) a PS–clay nanocomposite containing 12 wt % TBDO-MMT.

tially intercalated structures. The structures of the obtained PS–MMT nanocomposites were further confirmed with TEM (Fig. 2). In the TEM photographs, the layers of the hybrid appear as regions of alternating narrow, dark bands and light bands within the particle. The dark lines in the figure correspond to the silicate. For the nanocomposite containing 5 wt % TBDO-MMT [Fig. 2 (A)], the randomly stacked silicate layers, which were approximately 500 nm long and approximately 30–50 nm thick and consisted of approximately 10 parallel individual silicate layers, corresponding to the PS-containing galleries in agreement with the *d*-spacing observed by XRD (Fig. 1), were observed homogeneously in the continuous PS matrix. The PS/TBDO-MMT hybrid was a multilayered, sandwichlike material in which polymer chains were sandwiched between ultrathin sheets of organophilic MMT. With increasing TBDO-MMT loading, partial exfoliation occurred, and this was corroborated by TEM analysis [Fig. 2(B)]: both stacked (intercalated) and isolated (exfoliated) silicate layers could be observed. In general, there is competition between the viscosities of the intragallery and extragallery phases during *in situ* polymerization, so exfoliation is only possible when the intragallery polymerization is at least equal to, or faster than, the extragallery polymerization. In our experiments, the initiator concentration was kept the same, and so the viscosity of the extragallery phase decreased as the clay concentration in-

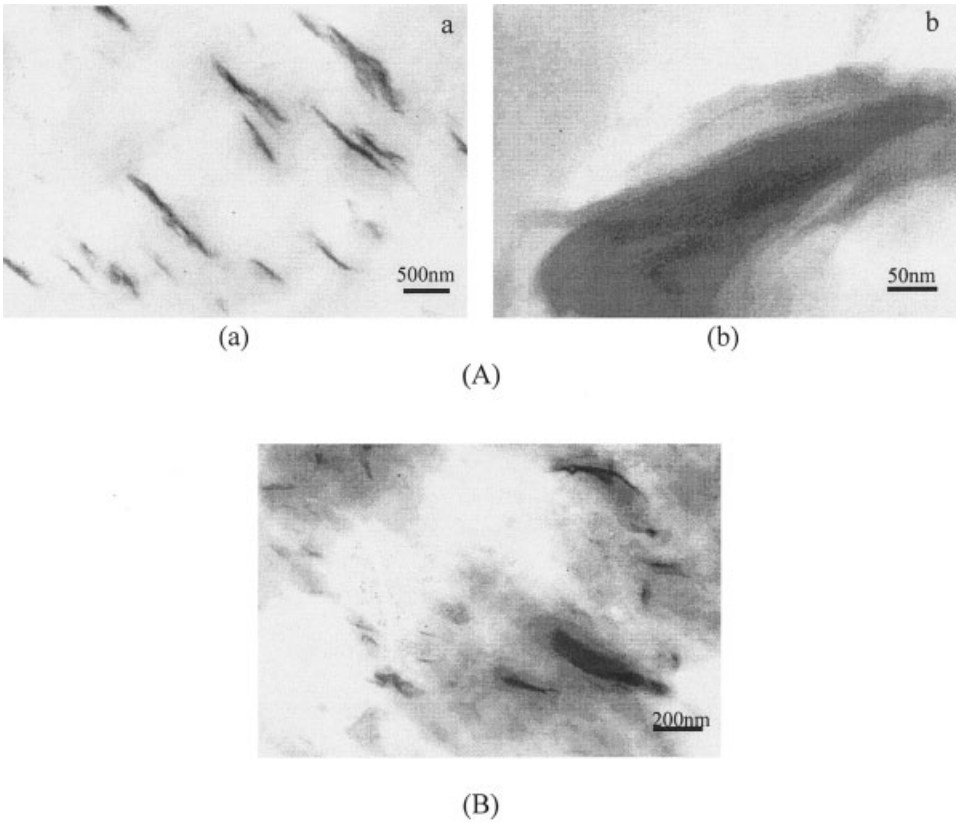

Figure 2 TEM micrographs of PS–clay nanocomposite: (A) 5 wt % TBDO-MMT [(a) general view and (b) intercalated structure] and (B) 12 wt % TBDO-MMT.

TABLE I
DSC Data of the PS–Clay Nanocomposites

TBDO-MMT content (wt %)	PS content (wt %)	T_g (°C)
0	100	97.6
1	99	97.1
3	97	94.2
5	95	91.4
8	92	89.0
12	88	84.6

creased because of the reduction of the polymer chain, which was hindered by the silicate platelets. However, the initiator concentration almost did not change in the intragallery phase, so the viscosity of the intragallery phase was higher than that of the extragallery, and it also facilitated the formation of an exfoliated and partially intercalated structure. The results require further investigation.

Table I provides T_g results for PS and PS/TBDO-MMT nanocomposites. T_g of the PS/TBDO-MMT nanocomposites decreased with increasing MMT loading. Fu and Qutubuddin[13] and Chang et al.[17] observed similar results. The former attributed this to two factors: the high viscosity of organophilic MMT dispersed in the styrene monomer affected the diffusion of initiator molecules, and MMT platelets blocked chain propagation during polymerization. This led to the reduction of T_g and M_w of PS. The latter considered organophilic MMT as a plasticizer for PS.[17] In our experiments, we think TBDO-MMT acted as a plasticizer in the obtained nanocomposites, and the exfoliated and partially intercalated structure may have had a more effective plasticizing effect; therefore, T_g of the exfoliated and partially intercalated structure was lower than that of pure PS and intercalated PS

To further investigate the factors affecting the properties of PS–clay nanocomposites, we measured the number-average molecular weight (M_n), M_w, and M_w/M_n values of the samples by GPC. The results are given in Table II. The molecular weight increased with an increasing TBDO-MMT load in comparison with

TABLE II
M_w Values of the PS–Clay Nanocomposites

TBDO-MMT content (wt %)	PS content (wt %)	$M_n \times 10^{-4}$ (g/mol)	$M_w \times 10^{-4}$ (g/mol)	M_w/M_n
0	100	11.0	28.1	2.55
1	99	11.2	28.1	2.51
2	98	14.7	31.5	2.33
3	97	18.4	39.3	2.14
5	95	22.9	47.2	2.06
8	92	22.0	43.6	1.98
10	90	17.3	39.9	2.31
12	88	16.5	37.7	2.28

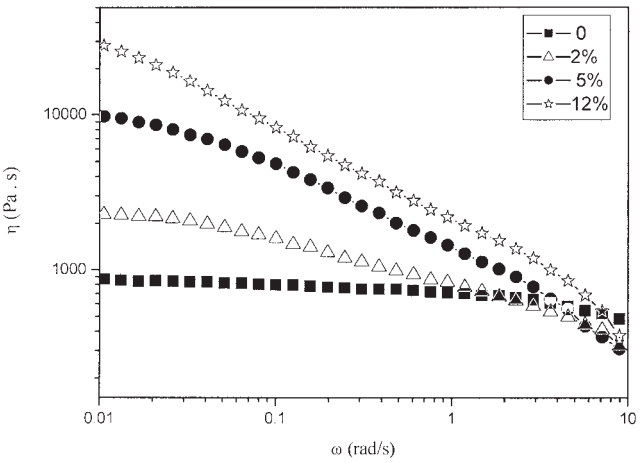

Figure 3 η versus ω for PS and PS/TBDO-MMT melts.

that of virgin PS. When the concentration of TBDO-MMT was approximately 5 wt %, the molecular weight reached the maximum. With a further increase

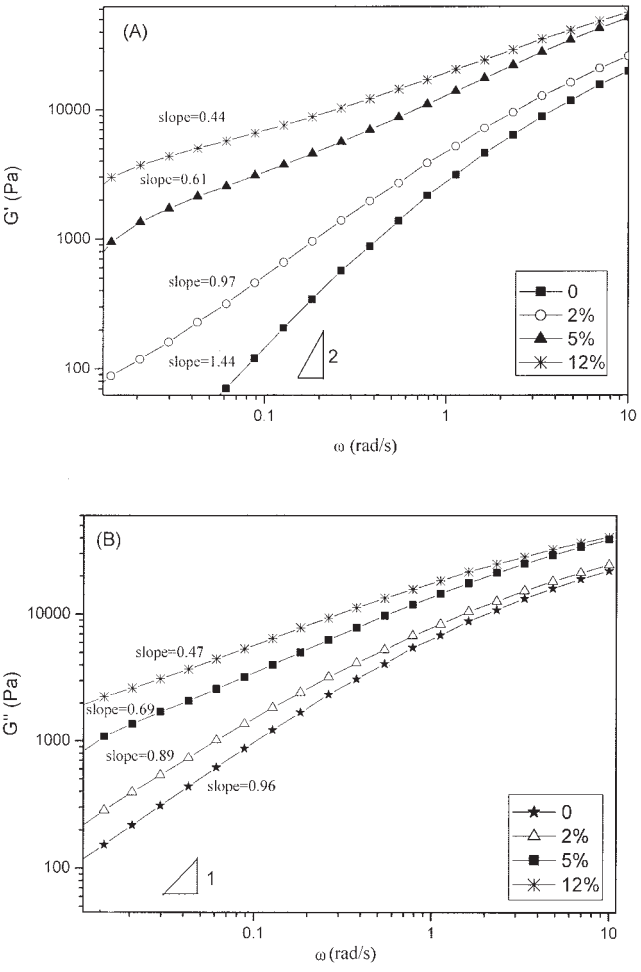

Figure 4 Plots of (A) log G' versus log ω and (B) log G'' versus ω at 250°C for pure PS and PS/TBDO-MMT nanocomposites.

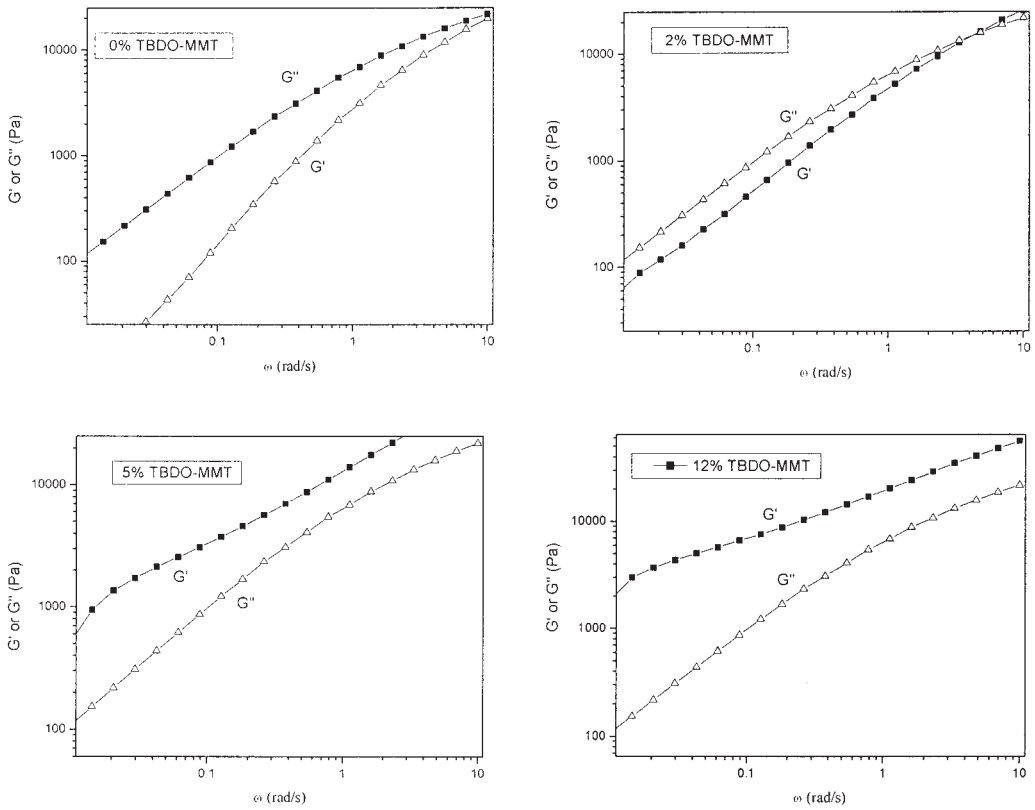

Figure 5 G' and G'' versus ω for PS and PS/TBDO-MMT nanocomposites.

in the concentration of TBDO-MMT, the molecular weight slightly decreased, but it was still higher than that of virgin PS. This indicated that the reduction of T_g could be attributed to neither the high viscosity of the organophilic MMT styrene dispersion, which affected the diffusion of initiator molecules, nor the blocking of chain propagation by MMT platelets in our system. The reduction of T_g might be attributed to the plasticization of PS by TBDO-MMT. When the organophilic MMT concentration was high enough, it might have had some effects on the diffusion of initiator molecules and the blocking of chain propagation by MMT platelets, and the molecular weight decreased. In the TEM images, the data for the exfoliated and partially intercalated structure could be observed with increasing TBDO-MMT content. Although the polydispersity initially decreased and then slightly increased with an increase in the clay loading, the change in the value was very small in comparison with the work of Noh and Lee.[18,19] This may be because the clay loading was less than 12 wt %, and so all the samples had similar M_w/M_n values.

Because of the need to understand the influence of various shear environments on polymer nanocomposite systems, the rheological behavior of nanocomposites as received considerable attention over the past several years.[21–25] Figure 3 shows logarithmic plots of η versus ω at 250°C for virgin PS and PS/TBDO-MMT nanocomposites. With an increasing TBDO-MMT concentration, η increased. This may be attributed to the increasing molecular weight and TBDO-MMT concentration of the PS/TBDO-MMT nanocomposites. A similar result was detected by GPC. There were also significant differences in the low-frequency oscillatory data between the pure PS and the three nanocomposites. The non-Newtonian behavior of the PS/TBDO-MMT nanocomposites increased with increasing TBDO-MMT contents. The transitions from the Newtonian plateau to the non-Newtonian regime shifted to a lower frequency as the TBDO-MMT concentration increased. The pure PS exhibited a wide Newtonian regime for frequencies less than 3 rad/s. The low-frequency response for the PS/2 wt % TBDO-MMT nanocomposite showed Newtonian-like behavior only at frequencies less than 0.1 rad/s. The Newtonian plateau for nanocomposites with higher TBDO-MMT (12%) was hardly observed. Many factors, such as the molecular weight distribution (MWD), can enhance non-Newtonian behaviors. However, MWD was not a key factor in this case because all the samples had similar M_w/M_n values. Therefore, the strong non-Newtonian behaviors were ascribed to the intercalative or exfoliated structure in the nanocomposites.

Figure 4 presents, with logarithmic plots of G' and G'' versus ω, the effect of the concentration of TBDO-MMT on the dynamic linear viscoelastic properties of

the PS/TBDO-MMT nanocomposites. G' for the PS/TBDO-MMT nanocomposites increased with an increasing TBDO-MMT load. The increase in the elastic modulus may have resulted from an improvement in the molecular weight and from the interactions between the polymer chains and clay. This result was consistent with that of GPC for 2 and 5 wt % PS/TBDO-MMT nanocomposites. G' for the 12 wt % sample was the highest, although its molecular weight was not the largest. This was due to the stronger interactions between the polymer molecules and the clays at high clay concentrations. Such interactions were also shown by the dependence of the dynamic moduli on the oscillatory frequency. When the polymer chains were fully relaxed, they exhibited characteristic homopolymer-like terminal behavior (i.e., $G' \propto \omega^2$ and $G'' \propto \omega$). The slope of G' versus ω in the log–log plot for pure PS was 1.1 at the low-frequency regime; this deviated from the terminal slope (2.0) of the monodispersed linear polymer and indicated a polydisperse molecular weight. The terminal zone slopes for the PS/TBDO-MMT nanocomposites decreased with an increasing TBDO-MMT load. The differences in the slopes may be attributed to the differences in the extent of intercalation or exfoliation. A larger extent of intercalation or exfoliation led to more solidlike behavior. The silicate layers in the hybrids were highly anisotropic, with lateral dimensions of 100–1000 nm, and even when separated by large distances (i.e., when delaminated), they could not be placed completely randomly in the sea of the polymer. Furthermore, the majority of the polymer chains in the hybrids were tethered to the surface of the silicate layers. The PS/12% TBDO-MMT nanocomposite had partial intercalation and partial exfoliation, and so its terminal zone slope was only 0.44; this was consistent with the XRD and TEM results. These trends were similar to those observed for other polymer–MMT nanocomposites.[21,22] The frequency dependence of G'' also monotonically increased with an increasing silicate loading at all frequencies. The low-frequency-regime frequency dependence of G'' decreased monotonically with an increasing TBDO-MMT loading from $\omega^{0.95}$ to $\omega^{0.47}$. As a result, the nanocomposites provided polydispersity over the entire frequency region. As shown in Figure 5, these data demonstrate that pure PS was less elastic ($G' < G''$), whereas the nanocomposites were more elastic ($G' > G''$). This may be related to intercalation or exfoliation.

The thermal stability of a material is usually assessed by thermogravimetric analysis (TGA), in which the sample mass loss due to volatilization of degraded byproducts is monitored as a function of a temperature ramp. When the heating is operated under an inert gas flow (nitrogen), nonoxidative degradation occurs, whereas the use of air or oxygen allows the oxidative degradation of the sample to be followed.

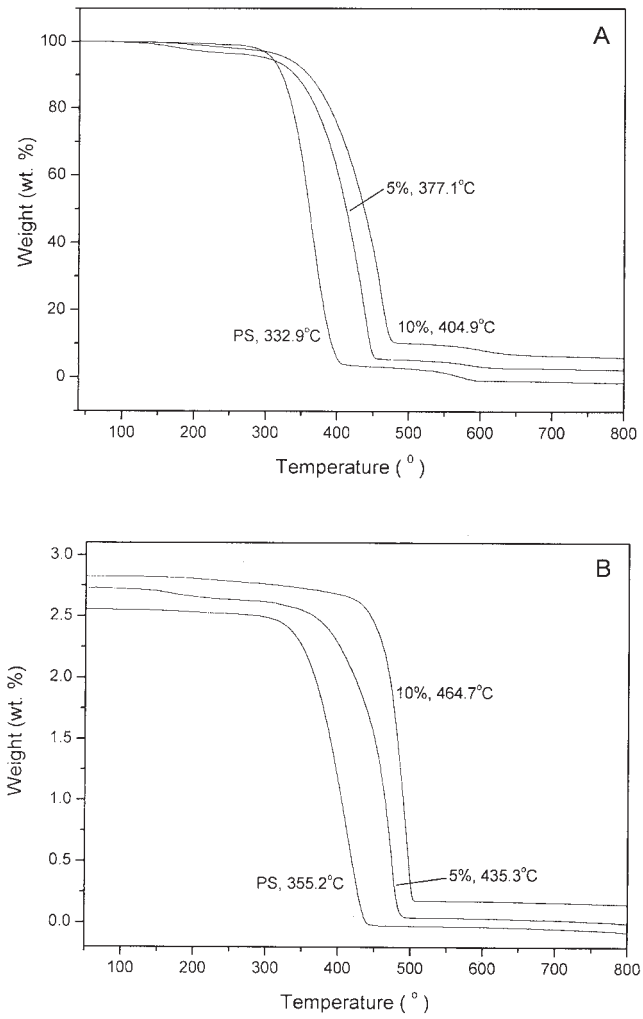

Figure 6 TGA thermograms for PS–clay nanocomposites under (A) an air atmosphere and (B) a nitrogen atmosphere (PS = virgin polystyrene, 5% = nanocomposite containing 5 wt % TBDO-MMT, 10% = nanocomposite containing 10 wt % TBDO-MMT).

Figure 6 shows TGA thermograms of virgin PS and PS–clay nanocomposites under air and nitrogen atmospheres. The TGA curve of the composites shows delayed decomposition in comparison with that of virgin PS, and with an increase in the TBDO-MMT load, the decomposition onset temperature of the composites shifted toward the higher temperature. Figure 6 also shows that the nanocomposite (containing 10 wt % TBDO) had decomposition temperatures 70 and 110°C higher than those of virgin PS under air and nitrogen flow, respectively. This indicated that the PS–clay nanocomposite had much higher thermal stability than virgin PS under thermodegradation and thermooxidative degradation. The much better thermal stability may be attributed to the hindrance of the diffusion of the volatile decomposition products, which resulted from the confinement of PS polymer chains between MMT layers, as well as the MMT

surface–polymer interactions in the nanostructured hybrid of PS and TBDO-MMT. Therefore, an improvement in the thermal stability will lead to the better service performance of the hybrid composite at an elevated temperature.

CONCLUSIONS

The results of this study show that the structural affinity between the styrene monomer and the organic group of organophilic MMT is an important factor for the preparation of nanocomposites. The structural affinity in the PS/TBDO-MMT hybrid can be attributed to the presence of a benzyl unit in the alkyl ammonium cation of TBDO-MMT, which is similar in structure to the styrene monomer. Therefore, TBDO-functionalized MMT has strong swelling ability and forms a viscous gel in styrene. Intercalated PS nanocomposites were successfully synthesized by bulk polymerization. The PS–clay nanocomposites exhibited higher molecular weights and a higher thermal stability.

The authors thank Jie Yin (School of Chemistry and Chemical Engineering, Shanghai Jiao Tong University) for enthusiastic discussions.

References

1. LeBaron, P. C.; Wang, Z.; Pinnavaia, T. J. Appl Clay Sci 1999, 15, 11.
2. Alexandre, M.; Dubois, P. Mater Sci Eng R 2000, 28, 1.
3. Theng, B. K. G. The Chemistry of Clay–Organic Reactions; Wiley: New York, 1974.
4. Ogawa, M.; Kuroda, K. Bull Chem Soc Jpn 1997, 70, 2593.
5. Kojima, Y.; Usuki, A.; Kawasumi, M.; Okada, A.; Fukushima, Y.; Karauchi, T.; Kaigaito, O. J Mater Res 1993, 8, 1185.
6. Messerasmith, P. B.; Giannelis, E. P. Chem Mater 1994, 6, 1719.
7. Friedlander, H. Z.; Grink, C. R. J Polym Sci Part B: Polym Lett 1964, 2, 475.
8. Blumstein, A. J Polym Sci Part A: Gen Pap 1965, 3, 2653.
9. Kato, C.; Kuroda, K.; Takahara, H. Clay Clay Miner 1981, 29, 294.
10. Akelah, A.; Moet, A. J Mater Sci 1996, 31, 3589.
11. Vaia, R.; Ishii, H.; Giannelis, E. Chem Mater 1996, 8, 1728.
12. Doh, J. G.; Cho, I. Polym Bull 1998, 41, 511.
13. Fu, X.; Qutubuddin, S. Mater Lett 2000, 42, 12.
14. Yoon, J. T.; Jo, W. H.; Lee, M. S.; Ko, M. B. Polymer 2001, 42, 329.
15. Okamoto, M.; Morita, S.; Taguchi, H.; Kim, Y. H.; Kotada, T.; Tateyama, H. Polymer 2000, 41, 3887.
16. Grim, R. E. Clay Mineralogy; McGraw-Hill: New York, 1968.
17. Tseng, C. R.; Wu, J. Y.; Lee, H. Y.; Chang, F. C. Polymer 2001, 42, 10063.
18. Lee, D. C.; Jang, L. W. J Appl Polym Sci 1996, 61, 1117.
19. Noh, M. W.; Lee, D. C. Polym Bull 1999, 42, 619.
20. Cho, J. W.; Paul, D. R. Polymer 2001, 42, 1083.
21. Krishnamoorti, R.; Giannelis, E. P. Macromolecules 1997, 30, 4097.
22. Fornes, T. D.; Yoon, P. J.; Keskkula, H.; Paul, D. R. Polymer 2001, 42, 9929.
23. Graebling, D.; Muller, R.; Palierne, J. F. Macromolecules 1993, 26, 320.
24. Lee, H. M.; Park, O. O. J Rheol 1994, 38, 1405.